RSC Advances

PAPER

View Article Online
View Journal | View Issue

Cite this: *RSC Adv.*, 2021, **11**, 31084

Electrospinning preparation and near-infrared absorption properties of a silica/cesium tungsten bronze micro–nano fiber membrane

Yilong Song,[a] Fang Zhao,*[a] Zhizun Li,[a] Zhaogang Cheng[a] and Hongjing Wan[b]

Silica/cesium tungsten bronze (SiO_2/Cs_xWO_3) composite micro–nano fiber membranes were prepared by the co-precursor electrostatic spinning method using cesium chloride, tungsten powder and tetraethyl orthosilicate as raw materials. TGA, XRD, FT-IR, XPS, SEM and ultraviolet-visible-near red spectrophotometry were used to analyze the thermal decomposition process, phase composition, microscopic morphology and near-infrared absorption properties of the product. Studies have shown that as the ratio of Cs/W of raw materials increases, the crystallinity of Cs_xWO_3 in the product increases first and then decreases. When n(Cs)/n(W) reaches 0.5, its crystallinity is the most complete; similarly, calcination also contributes to the crystallization of $Cs_{0.33}WO_3$, but high temperatures above 800 °C will also destroy its crystal structure. The study found that after calcination at 700 °C, the fiber membrane with a Cs/W atomic ratio of 0.5 has the best infrared absorption performance. The average absorbance of near-infrared light at 780–2500 nm is 1.5, which is 5.56 times that of the pure SiO_2 fiber membrane. The tensile strength reaches 2.4 MPa, which can meet practical requirements. This research provides a basis for the development of flexible solar shading materials under complex outdoor conditions.

Received 14th August 2021
Accepted 15th September 2021

DOI: 10.1039/d1ra06157g

rsc.li/rsc-advances

Introduction

As the concept of environmental protection and energy saving continues to gain popularity, various high-performance thermal insulation materials have been invented to shield excess heat from sunlight. The SiO_2 micro–nano fiber membrane has attracted great attention worldwide for having stable properties, low thermal conductivity and excellent flexibility.[1] Recent studies show that SiO_2 is almost completely transparent to near-infrared light (wavelength of 780–2500 nm), the main heat source in solar radiation, which will make energy accumulate inside the material and increase the temperature sharply (Fig. 1).[2,3] Therefore, improving the shielding ability of SiO_2 micro–nano fiber membranes for near-infrared radiation is an important topic in the current research of thermal insulation materials.

Adding sunscreens to heat insulation materials is an effective means to block near-infrared radiation. According to different working mechanisms, sunscreens can be divided into reflective and absorbing types.[4] Reflective sunscreens are based on the fact that the incident frequency of sunlight is greater than the vibration frequency of the particles themselves, which causes the particles to reflect energy in the infrared band.[5] The absorbing sunscreens use ion resonance on the surface of the sunscreen particles to make it absorb in the near-infrared region.[6] Cs_xWO_3 is an emerging high-performance absorbing infrared sunscreen, whose basic structural unit is formed by [WO_6] octahedrons connected by common vertices. The Cs^+ whose radius is slightly bigger than the hexagonal hole of tungsten bronze could be easily filled into the hole of tungsten bronze and is not easy to escape, thereby triggering the small polaron effect. The above-mentioned characteristic enables it to shield almost all light of the near-infrared wavelengths (750–2500 nm), and show better heat shielding performance than indium tin oxide (ITO) and antimony tin oxide (ATO). Therefore, Cs^+ has better application potential and research value in the field of thermal insulation materials. Xu *et al.*[7] analyzed the optical properties of $Cs_{0.33}WO_3$ based on first-principles theory within the framework of density functional theory, and theoretically proved its excellent near-infrared absorption performance. In the application field, researchers have explored a series of preparation processes, using water-based resin,[8] SiO_2 sol[9] and PMMA[10] as the matrixes, and transparent glass as the carrier to obtain a variety of high-temperature near-infrared shielding glass plates with Cs_xWO_3. Zhang *et al.* used coaxial electrospinning technology to prepare a core–shell-structured nano-smart fiber with cesium tungsten bronze on the shell, which can effectively shield the near-infrared radiation from sunlight.[11] Related studies have shown that the uniform dispersion of Cs_xWO_3 particles in the matrix has a greater impact on the infrared shielding performance of the material.[12] At present, the uniform dispersion process of Cs_xWO_3 particles is still a problem, and the poor adaptability of rigid insulating glass to complex environments also affects the practical value of the material.

[a]*Department of Vehicle and Electrical Engineering, PLA Army Engineering University, Shijiazhuang Campus, Shijiazhuang 050003, China. E-mail: zhaofang19821106@163.com*

[b]*Hebei Huanrui Chemical Co., Ltd., Shijiazhuang 050003, China*

In this paper, tungsten powder and cesium chloride were used as raw materials to prepare Cs_xWO_3 sol with the sol–gel method. Cs_xWO_3 sol was then mixed with tetraethyl orthosilicate hydrolysate. The SiO_2/Cs_xWO_3 composite fiber membrane (SCF) was prepared by electrostatic spinning method combined with heat treatment technology. The infrared shielding performance of the material was evaluated by the near-infrared absorbance. The effects of different Cs/W doping ratios and calcination temperatures on the phase composition and infrared absorbance of SCF were discussed, and the near-infrared shielding mechanism of SCF was analyzed and discussed. This study provides an experimental basis for the preparation of flexible near-infrared shielding materials with great environmental adaptability.

Experimental

Materials

Hydrogen peroxide (H_2O_2, 30 wt%) was purchased from Tianjin Damao Chemical Reagent Co., Ltd., China. Tetraethyl orthosilicate (TEOS), ethanol absolute and oxalic acid ($H_2C_2O_4$) were purchased from Tianjin Yongda Chemical Co., Ltd., China. Tungsten powder, cesium chloride and tetrabutylammonium chloride were purchased from Xiya Chemical Reagent Co., Ltd., China. All chemicals were of analytical grade and were used as received without further purification.

Sample preparation

Uniformly mix the TEOS and ethanol absolute at a mass ratio of 2 : 1, and use oxalic acid as a catalyst. Solution A was obtained after 8 hours of magnetic stirring of the above mixture at room temperature. 0.1 g of tungsten powder was dissolved in 1.3 g of 30 wt% H_2O_2 solution, stirred for 3.5 h and then filtered, and the filtrate was stirred in a water bath at 80 °C for 5 h to obtain a yellow solution. According to the ratio of Cs/W atomic substance (Cs/W = 0.1, 0.2, 0.3, 0.4, 0.5 and 0.6, respectively), CsCl of corresponding mass was added, and Cs_xWO_3 sol was obtained after stirring. The Cs_xWO_3 sol was mixed with solution A, and the organic branched salt tetrabutylammonium chloride was added to improve the conductivity of the solution. After heating in a water bath at 60 °C for 2 h, a spinning precursor solution was obtained.

The SiO_2/Cs_xWO_3 micro–nano fiber membranes were prepared with a self-made electrospinning equipment in the laboratory. The parameters of the electrospinning process are: at room temperature, the voltage is 17 kV; the needle is a 19 G stainless steel needle; the distance between the needle and the receiving plate is 20 cm, and the precursor fluid flow rate is 0.1 mL h^{-1}. According to different ratios of Cs/W in the precursor solution, the fiber membranes were numbered as $SCF_{0.1}$–$SCF_{0.6}$.

The fiber membrane prepared through the above electrospinning process was placed in a tube furnace, heated to 500 °C, 600 °C, 700 °C and 800 °C respectively at a rate of 2 °C min^{-1} in a nitrogen atmosphere, and calcined and kept for 2 h, and then cooled to room temperature with the furnace.

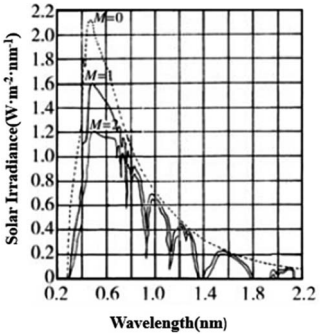

Fig. 1 Distribution of light of different wavelengths in the solar spectrum.[2]

Characterization

The synthesis process of the sample was detected by thermal gravimetric analysis (TGA, SDT-Q600, TA, USA). The phase composition of the sample was detected by X-ray diffraction (XRD, XD6, Purkinje, China). The infrared spectrum of the sample was analyzed by Fourier transform infrared spectrometer (380, Nicolet, USA). The microscopic morphology of the sample was observed with a field emission scanning electron microscope (SEM, SU-8010, Hitachi, Japan). The infrared absorbance of the sample was analyzed using a UV-visible-near infrared spectrophotometer (Shimadzu UV-3600, Japan): the wavelength range is 200–2500 nm, the scanning speed is 240 nm min^{-1}, and the slit width is 2 nm. The tensile strength of the sample was analyzed using a tensile testing machine (INSTRON 5982, USA).

Results and discussion

Fig. 2 is the DSC-TGA curve of the SCF membrane. As can be seen from the curve, the heat treatment process of the fiber membrane can be divided into three stages: the first stage was from room temperature to 197 °C, during which the mass loss of the sample was about 18.3%, and the DSC curve had an endothermic peak at 105 °C. The second stage was 197–500 °C, and the weight loss rate of this part was about 3.7%. We think this is

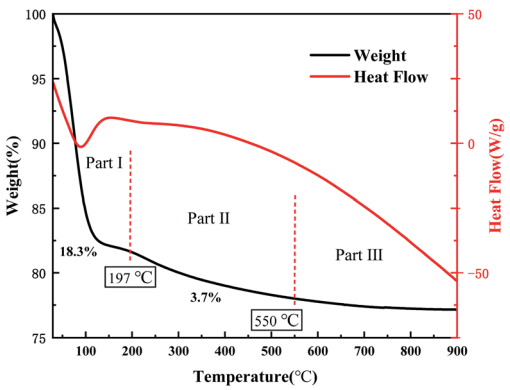

Fig. 2 DSC-TGA curves of $SCF_{0.5}$ membrane.

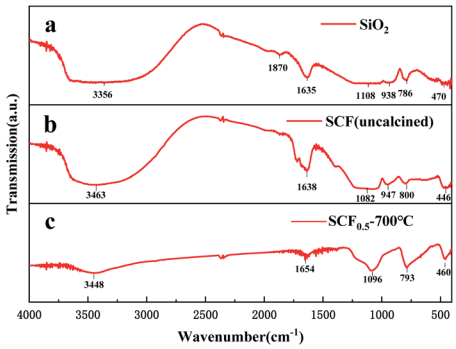

Fig. 3 FTIR spectra of (a) SiO_2 (uncalcined), (b) $SCF_{0.5}$ (uncalcined) and (c) $SCF_{0.5}$ (calcined at 700 °C).

related to the decomposition of raw materials such as oxalic acid and tetrabutylammonium chloride. In addition, the polycondensation dehydration between silica networks and the decomposition of hydrated tungsten oxide would also cause a small amount of quality loss.[13] The third stage was above 500 °C, the curve tended to be stable, the thermal decomposition process was over, and the Cs_xWO_3 crystal growth stage started. Therefore, in order to fully crystallize Cs_xWO_3 in the product, the calcination temperature should be set above 500 °C.

In order to further characterize the structure of the sample, FT-IR tests were performed on uncalcined SiO_2, SCF and SCF calcined at 700 °C. The results are shown in Fig. 3. The three curves all showed a strong absorption peak near 3450 cm^{-1} and 1640 cm^{-1}, being the antisymmetric stretching vibration peak of –OH and the bending vibration peak of H–O–H, respectively. This is caused by the product adsorbing water in the air. The broad and strong absorption peak near 1100 cm^{-1} was the Si–O–Si antisymmetric stretching vibration peak, the one near 800 cm^{-1} was the Si–O stretching vibration peak, and that near 460 cm^{-1} was the Si–O–Si bending vibration peak.[14] The absorption peaks of curves a and b near 940 cm^{-1} were Si–OH stretching vibration peaks. After calcination, this peak disappeared in curve c, indicating that the SiO_2 network had undergone polycondensation and the Si–OH bond was converted into Si–O–Si bond. In addition, the curve c had a higher absorption peak at 1000–500 cm^{-1} due to the absorption of Cs_xWO_3 in the near-infrared region, indicating that the sample had good near-infrared shielding ability after calcination at a high temperature. No other groups related to Cs^+ appeared in the curve, indicating that Cs^+ had entered the lattice of WO_3.[8]

Fig. 4 shows the XRD diffraction patterns of different samples ($SCF_{0.1}$–$SCF_{0.6}$) calcined at 700 °C with a Cs/W atomic ratio between 0.1 and 0.6. It can be seen from the figure that the diffraction curves of samples $SCF_{0.1}$ and $SCF_{0.2}$ had relatively low diffraction peaks when 2θ = 22.7°, 24° and 27.7°. Comparing the PDF cards of JCPDS 05-0388 and JCPDS 83-1344, we can find that they belonged to the (001) and (110) crystal planes of WO_3 and the (200) crystal plane of $Cs_{0.33}WO_3$, respectively. It shows that the product was in a three-phase coexistence state of amorphous SiO_2, WO_3 and $Cs_{0.33}WO_3$ at this ratio, but due to insufficient Cs^+ concentration, the crystallinity of $Cs_{0.33}WO_3$ was not high. With the increase of the atomic ratio of Cs/W to above 0.3, the diffraction peaks corresponding to $Cs_{0.33}WO_3$ crystals in the XRD curve gradually became sharper, and the characteristic diffraction peaks representing WO_3 all disappeared. At this time, [WO_6] octahedral channels had been fully embedded by Cs^+, which effectively increased the carrier concentration in the conduction band and improved the near-infrared absorption performance of the material. Although sufficient Cs^+ source is of great significance to the perfection of $Cs_{0.33}WO_3$ crystal form, there is also a saturation value for the Cs^+ concentration. Judging from the sharpness of the diffraction peaks in the sample XRD curve, when n(Cs)/n(W) reached 0.5, the $Cs_{0.33}WO_3$ in the sample had the best crystal structure. With the further increase of Cs^+ concentration, the crystallinity of $Cs_{0.33}WO_3$ in the sample decreased. This may be due to the presence of excessive Cs^+ and Cl^- which caused the local electric potential in the spinning precursor to change, and then the colloidal particles in the precursor to over-aggregate and hinder the growth of crystals.

In order to explore the effect of heat treatment temperature on the phase composition of the SCF membrane, XRD analysis was performed on the calcined products of $SCF_{0.5}$ at different temperatures, and the diffraction curve is shown in Fig. 5. There is no diffraction peak attributed to SiO_2 crystals in the curve, indicating that SiO_2, as the matrix material of the fiber, is always in an amorphous state below 800 °C, which is the basis for the good flexibility of the SCF membrane. In the diffraction curve of

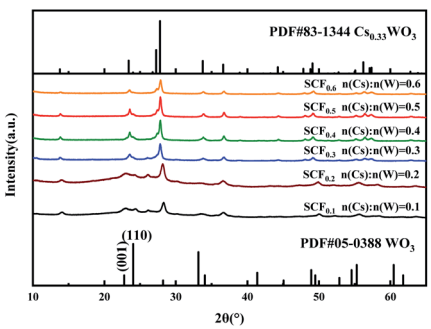

Fig. 4 XRD patterns of SCF membrane with different Cs/W ratios calcined at 700 °C.

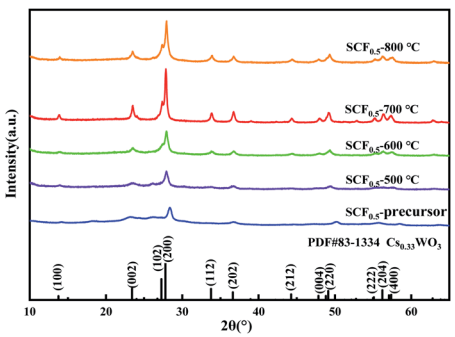

Fig. 5 XRD patterns of $SCF_{0.5}$ after heat treatment at different temperatures.

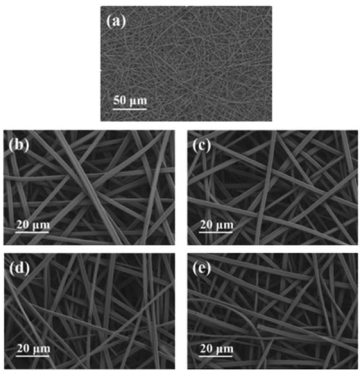

Fig. 6 (a) SEM images of precursor $SCF_{0.5}$ membrane, (b) $SCF_{0.5}$-500 °C (c) $SCF_{0.5}$-600 °C (d) $SCF_{0.5}$-700 °C and (e) $SCF_{0.5}$-800 °C.

the uncalcined precursor SCF membrane, a low diffraction peak can be observed at $2\theta = 27.7°$. As mentioned earlier, it belongs to the (200) crystal plane of $Cs_{0.33}WO_3$. It shows that Cs^+ spontaneously entered into the hexagonal lattice of $[WO_6]$ before heat treatment, and $Cs_{0.33}WO_3$ crystals were formed after drying. But at this time, the diffraction peak in the curve was relatively low, and the crystallization of $Cs_{0.33}WO_3$ was insufficient. As the calcination temperature increased, the driving force for promoting crystal growth increased, and the diffraction peaks in the curve gradually became sharper. When the heat treatment temperature reached 700 °C, sharp characteristic peaks were observed at $2\theta = 24.6°$, $27.7°$, $33°$ and $36°$, which are attributed to (002), (200), (112) and (202) planes of the $Cs_{0.33}WO_3$ crystal, respectively. In addition, the characteristic peak attributable to the $Cs_{0.33}WO_3$ (102) crystal plane at $2\theta = 27.2°$ in the figure was not obvious, which may be the result of the superposition of the dispersion peak of amorphous SiO_2 here. With the further rise of the heat treatment temperature, the intensity of the diffraction peak decreased at 800 °C. This may be due to the fact that the excessively high temperature caused Cs^+ to break away from the $[WO_6]$ lattice, which destroyed the crystal structure of $Cs_{0.33}WO_3$.

Fig. 6(a) is an electron micrograph of the uncalcined precursor $SCF_{0.5}$ membrane. It can be seen from the figure that the fibers had a three-dimensional network structure with uniform diameter and good continuity. After the $SCF_{0.5}$ membrane was calcined at 500 °C, 600 °C, 700 °C, and 800 °C in an N_2 atmosphere, the morphology of the product obtained is shown in Fig. 6(b–e). The fiber calcined at 500–700 °C can still maintain a three-dimensional network structure, and the surface of the fiber was smooth without cracks. After the calcination temperature was raised to 800 °C, a small amount of fiber breakage appeared in the field of vision. This is because the excessively high temperature provides more driving force for the growth of the $Cs_{0.33}WO_3$ lattice so that it has a higher surface energy, which macroscopically destroys the fiber continuity.

Fig. 7 shows the stress–strain curves of the sample after the $SCF_{0.5}$ membrane was calcined at different temperatures. As can be seen from the figure, a lower heat treatment temperature

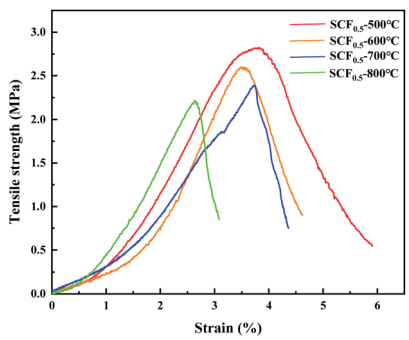

Fig. 7 The stress–strain curves of samples $SCF_{0.5}$-500 °C, $SCF_{0.5}$-600 °C, $SCF_{0.5}$-700 °C and $SCF_{0.5}$-800 °C.

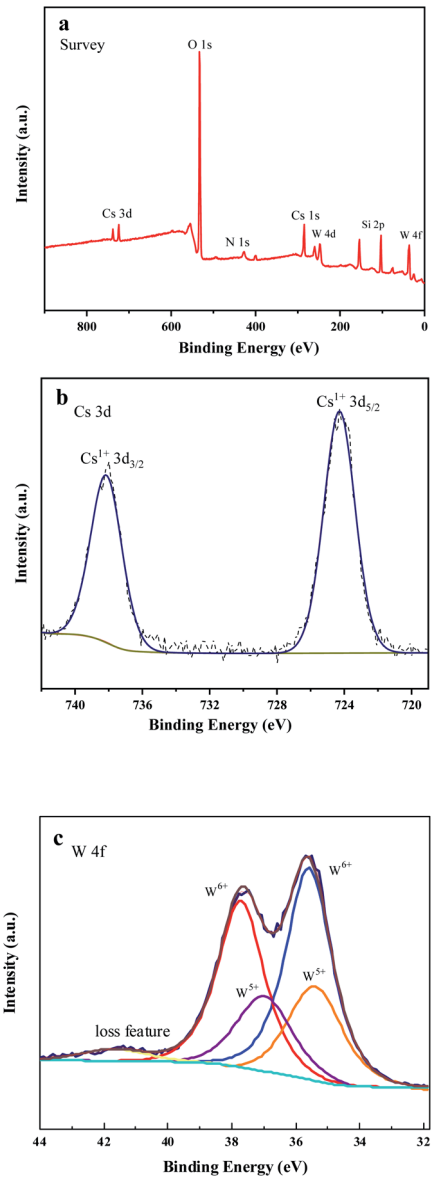

Fig. 8 (a) XPS survey spectrum (b) Cs 3d spectrum and (c) W 4f spectrum of $SCF_{0.5}$-700 °C.

helped the fiber membrane maintain good flexibility and strength. With the increase of the calcination temperature, the lattice structure of $Cs_{0.33}WO_3$ in the fiber grew excessively at high temperatures, destroying the molecular chain in amorphous SiO_2, thereby reducing the toughness and strength of the fiber membrane.

Fig. 8(a–c) show the XPS survey spectrum, Cs 3d orbital spectrum and W 4f orbital spectrum of $SCF_{0.5}$-700 °C samples, respectively. All peaks were calibrated with C 1s adsorption carbon C–C/C–H binding energy of 284.8 eV, and Avantage software was used to perform peak fitting of XPS data. Analyzing Fig. 8(a), it can be seen that there were binding energy peaks of Cs, W, O, Si and N in the sample. Among them, the peak of N originated from the pollution of N_2 during the calcination process, which had little effect on the performance of the product. The obtained results indicate that a relatively pure $SiO_2/Cs_{0.33}WO_3$ product has been prepared, which is in good agreement with the XRD test results. Fig. 8(b) shows the diffraction double peaks of the Cs 3d orbital, in which the peak at 724 eV was caused by the Cs–O bond, indicating that Cs had successfully entered the hexagonal channels of tungsten bronze.[15] By performing peak splitting processing on W 4f orbital, we can obtain W 4f split peak fitting spectra (Fig. 8(c)). It can be seen from the figure that the splitting peaks of W 4f are composed of W^{5+} double peaks at 34.28 eV and 35.98 eV and W^{6+} double peaks at 35.58 eV and 37.68 eV. The addition of Cs changed the valence of some W ions, which led to the transfer of electrons between W in different valence states, improving the near-infrared absorption performance of the SCF membrane.[16]

Absorbance is a physical quantity used to evaluate the process of light being absorbed. In a certain waveband, the greater the absorbance of an opaque object, the stronger the shielding effect of light in this waveband. Fig. 9 shows the infrared absorption spectra of pure SiO_2 fiber membrane and $SCF_{0.5}$ samples calcined at different temperatures. It can be seen from the figure that pure SiO_2 had almost no absorption of light with a wavelength of less than 1400 nm. After being doped with $Cs_{0.33}WO_3$, the precursor fiber membrane had significantly improved optical absorption performance, and the average absorbance in the near-infrared band (780–2500 nm) increased from 0.27 to 0.89. After calcination at 500–800 °C, the average absorbance of $SCF_{0.5}$ membrane was 1.32, 1.46, 1.5 and 1.34, respectively. As can be seen from the comparison of Fig. 5 and 9, the near-infrared absorption performance of SCF membrane is closely related to the crystallinity of $Cs_{0.33}WO_3$ crystal. $SCF_{0.5}$-700 °C has the best crystallinity and near-infrared absorption. This is considered to be the result of the combined effect of the small polaron on the surface of the $Cs_{0.33}WO_3$ particles in the membrane and the plasmon resonance effect.[17] The addition of Cs^+ made the $[WO_6]$ tunnel contain a large number of free carriers, which are restricted to the position of W under the influence of the lattice energy, and produce small polarons on the surrounding lattice. The small polaron transitioned between different W positions and absorbs light in the near-infrared band.[18] In addition, a large number of carriers gave $Cs_{0.33}WO_3$ some metal-like properties, and the electron clusters formed by a large number of free electrons can be regarded as plasma. When the frequency of the incident light was close to the natural frequency of the plasma, strong coupling would occur, resulting in a localized surface plasma wave. The energy in the plasma wave was absorbed by the material in the process of propagation, which acted as a shield for the near-infrared rays.[19]

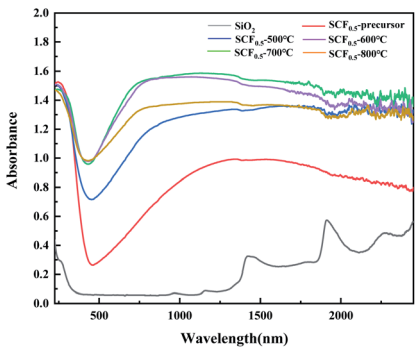

Fig. 9 Pure samples of SiO_2 and infrared $SCF_{0.5}$ absorbance spectrum at different temperatures.

Conclusions

In summary, SCF micro–nano fiber membranes with good near-infrared absorption properties were prepared by the sol–gel-electrospinning method. Based on the small polaron and plasmon resonance effect of the new near-infrared absorbent $Cs_{0.33}WO_3$, combined with the extremely low thermal conductivity of the SiO_2 fiber membrane, the comprehensive thermal insulation capacity of the composite fiber membrane is optimized. At the same time, the uniform mixing of the $Cs_{0.33}WO_3$ sol and the spinning precursor improves the dispersion effect of the sunscreen particles in the matrix material. After calcination at 700 °C, the SCF membrane with a Cs/W atomic ratio of 0.5 ($SCF_{0.5}$-700 °C) has the best near-infrared absorption performance, and the average absorption of light in the 780–2500 nm band is 1.5. This kind of flexible thermal insulation material with good shielding performance to sunlight is of great significance to the thermal protection of outdoor storage facilities.

Author contributions

Yilong Song: writing – original draft, formal analysis, resources and visualization; Fang Zhao: project administration, supervision and funding acquisition; Zhizun Li: data curation; Zhaogang Cheng: data curation; Hongjing Wan: conceptualization.

Conflicts of interest

There are no conflicts to declare.

Acknowledgements

This work is supported by the Hebei Natural Science Fund of China (E2015506011), Innovation and Development Science Foundation of the PLA Army Engineering University

Shijiazhuang Campus (KYSZJQZL1910) and Shijiazhuang City Science and Technology Small and Medium-sized Enterprise Technology Innovation Fund Project (21SCX04002).

Notes and references

1 Y. S. Si, X. Mao, H. X. Zheng, J. Y. Yu and B. Ding, *RSC Adv.*, 2014, **5**(8), 6027–6032.
2 L. H. Zhao and Q. H. Tang, *Equip. Environ. Eng.*, 2017, **12**(14), 73–78.
3 E. Hummer, X. Lu, T. Rettelbach and J. Fricke, *J. Non-Cryst. Solids*, 1992, **145**(145), 211–216.
4 J. Jing, Master's thesis, Beijing University of Chemical Technology, 2018.
5 K. Conley, S. Moosakhani, V. Thakore, Y. Ge and T. Ala-Nissila, *Ceram. Int.*, 2021, **47**(12), 16833–16840.
6 Z. L. Wang, *Prog. Phys.*, 2009, **29**(3), 287–314.
7 Q. Xu, L. Xiao, J. Ran, R. Tursun, G. Zhou, L. Deng, D. Tang, Q. Shu, J. Qin and G. Lu, *J. Appl. Phys.*, 2018, **124**(19), 193102.
8 S. M. Wang, Master's thesis, Donghua University, 2018.
9 J. Y. Wu, Master's thesis, Beijing University of Chemical Technology, 2017.
10 J. Y. Yang, Y. T. Qiao, J. X. Liu, F. Shi and X. Y. Song, *J. Dalian Polytech. Univ.*, 2020, **4**, 296–301.
11 M. Zhang, L. Q. Yi, J. M. Yao and G. C. Zhu, Preparation method of nano smart fiber for heat storage, Chinese Patent, CN110067038A, 2019.
12 J. Liu, X. Qiang, S. Fei, S. Liu, J. Luo, B. Lei and F. Xiang, *Appl. Surf. Sci.*, 2014, **309**(aug. 1), 175–180.
13 F. Zhang, Y. B. Dong and F. C. Meng, *Spectrosc. Spectral Anal.*, 2016, **36**(04), 991–995.
14 H. S. Chen, Z. Y. Sun and J. C. Shao, *Bull. Chin. Ceram. Soc.*, 2011, **30**(04), 934–937.
15 H. Takeda and K. Adachi, *J. Am. Ceram. Soc.*, 2007, **90**(12), 3.
16 F. Shi, J. X. Liu, X. L. Dong, Q. Xu, J. Y. Luo and H. C. Ma, *J. Mater. Sci. Technol.*, 2014, **30**(4), 342–346.
17 K. Adachi and T. Asahi, *J. Mater. Res.*, 2012, **27**(6), 965–970.
18 J. Hu and R. G. Gordon, *Sol. Cells*, 1991, **30**(1–4), 437–450.
19 K. A. Willets and R. V. Duyne, *Annu. Rev. Phys. Chem.*, 2007, **58**(1), 267–297.